Investigation of collar properties on data-acquisition scheme for acoustic logging-while-drilling

Citation: Wang, Hua; Fehler, Mike; Tao, Guo and Wei, Zhoutuo. "Investigation of Collar Properties on Data-Acquisition Scheme for Acoustic Logging-While-Drilling." Geophysics 81, no. 6 (November 2016): D611–D624. © 2016 Society of Exploration Geophysicists

As Published: http://dx.doi.org/10.1190/GEO2016-0016.1

Publisher: Society of Exploration Geophysicists

Persistent URL: http://hdl.handle.net/1721.1/109152

Version: Final published version: final published article, as it appeared in a journal, conference proceedings, or other formally published context

GEOPHYSICS, VOL. 81, NO. 6 (NOVEMBER-DECEMBER 2016); P. D611–D624, 18 FIGS., 2 TABLES.
10.1190/GEO2016-0016.1

Investigation of collar properties on data-acquisition scheme for acoustic logging-while-drilling

Hua Wang[1], Mike Fehler[2], Guo Tao[3], and Zhoutuo Wei[4]

ABSTRACT

We have used the wavenumber integration, velocity-time semblance, and dispersion methods to investigate the influence of collar properties including velocities, density, and attenuation on acoustic logging-while-drilling wavefields. We have found that when the velocities of the collar wave and the P-wave of the formation are similar, they interfere. However, the interference disappears when the velocity difference increases. Having a collar with large velocities (especial large shear velocity) and density makes the direct P-velocity determination possible in a fast formation even without isolators. For a slow formation, the interference of the collar flexural wave with the formation flexural and leaky P-waves is slight for a dipole tool when collar velocities are large. For this case, the S velocity can be determined by the flexural formation wave at low frequency (approximately 2 kHz). Based on these observations, we propose that the measurement of the P- and S-velocities can be easier if the collar is made of an advanced composite material that has high compressional and shear velocities as well as density. This is a direct and easy change to implement and a new idea for an acoustic logging-while-drilling tool design.

INTRODUCTION

Logging-while-drilling (LWD) is a key technology for monitoring during drilling, for real-time data acquisition, and for geosteering in horizontal wells and highly deviated wells (Wang et al., 2009a). Drill collars occupy most of the space in a fluid-filled borehole and divide the borehole fluid into two thin-fluid columns (Byun and Toksöz, 2003; Wang et al., 2009b; Wang and Tao, 2011), which makes the wavefield in acoustic LWD (ALWD) different from that in acoustic wireline logging. The collar makes it more difficult to identify the modes that are sensitive to formation (Wang et al., 2013a, 2015). It is difficult to identify the P-wave in a fast formation because of the interference between it and the collar wave. The main method to eliminate the interference is by using a sound isolator on the tool, in which the isolator is set either between the sensors (receivers and source) and drill pipe to decouple the collar and formation waves (Varsamis et al., 1999) or between the source and receiver to attenuate the amplitude of the collar wave or change the travel path of the collar wave (Aron et al., 1994; Leggett et al., 2001). Usually, grooves are cut periodically in the inner (Kinoshita et al., 2010) or outer wall (Varsamis et al., 1999) of the collar, and they act together as an acoustic isolator between the source and receiver (Aron et al., 1997; Joyce et al., 2001). The flexural rigidity of the drill pipe is directly proportional to the mass of the drill pipe and the difference of the fourth power of the outer and inner radii (Poletto and Miranda [2004], p. 82). Grooves on the inside of the collar reduce the collar flexural rigidity less than those on the outer wall. Isolators are difficult to make due to the required complex structure of the grooves.

Another approach to aid the analysis of the formation-sensitive modes is to use a data processing method to eliminate the interference of the collar waves. For example, Wang et al. (2009b) propose a method for obtaining collar waves numerically in conjunction with limited physical calibration experiments that can completely eliminate the interference of the collar during the signal processing, thus eliminating the need for isolators on the collar. Zhan et al. (2010) obtain information about the formation wave by using the seismoelectric effect, but the electric signal was very weak.

With the help of the discrete wavenumber integration (DWI) method (Tang and Cheng, 2004) and slowness-time semblance

Manuscript received by the Editor 7 January 2016; revised manuscript received 8 July 2016; published online 13 September 2016.
[1]Formerly University of Petroleum (Beijing), SKL-PRP, Beijing, China; presently Massachusetts Institute of Technology, Earth Resources Laboratory, Cambridge, Massachusetts, USA. E-mail: wanghuaupc@126.com.
[2]Massachusetts Institute of Technology, Earth Resources Laboratory, Cambridge, Massachusetts, USA. E-mail: fehler@mit.edu.
[3]Formerly University of Petroleum (Beijing), SKL-PRP, Beijing, China; presently the Petroleum Institute of Abu Dhabi, Abu Dhabi, UAE. E-mail: taoguo@cup.edu.cn.
[4]China University of Petroleum (East China), Beijing, China. E-mail: weizhoutuo@163.com.

(Kimball and Marzetta, 1984), we investigate the effects of the velocities, density, and attenuation of the collar on the multipole ALWD wavefield and try to find the parameters of the collar that have the most influence on formation waves.

ALWD MODEL AND THE SIMULATION METHOD

Figure 1 is a schematic diagram of an ALWD model including the formation, outer fluid, collar, and inner fluid. The different ALWD source configurations are shown in Figure 1a (monopole source), 1b (dipole source), and 1c (quadrupole source). The gray and white portions of the ring source that are located on the collar denote the positive and negative phases of the source, respectively. Figure 1d shows a side view of the model showing the configuration of the multipole ring source and array receivers. The spacing between source and the nearest receiver is 3 m, and the axial receiver interval is 0.15 m.

Table 1 gives the parameters and geometries of the model we used for our simulations.

The complex 3D structure of the isolator will not be considered in this paper. Therefore, the wavenumber integration method for the symmetrical acoustic logging modeling can be used for the study (Tang and Cheng, 2004). For the simulation, multiple point sources will be set on the outer collar to approximate a ring source (Chen et al., 2010). Wang and Tao (2011) and Wang et al. (2015) show how to get the dispersion curves for different modes in the borehole from the wavenumber integration formulation by using a root-finding Newton-Raphson mode-search routine (Tang and Cheng, 2004).

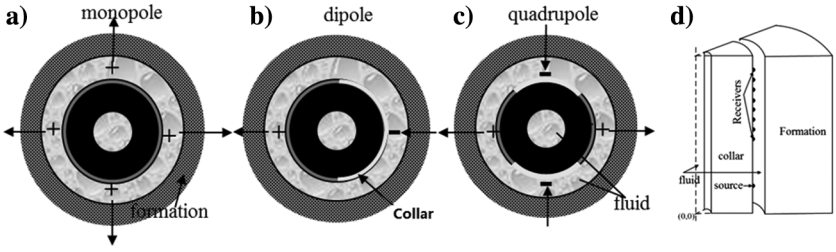

Figure 1. Schematic diagram of LWD acoustic model. (a-c) Top-down view of the model showing different ALWD sources and (d) side view of the model. Horizontal and vertical direction in (a-c) are x and y, respectively. Borehole axis in d) is z direction.

Table 1. Parameters for the LWD model. The values V_P and V_S are the velocity of the P- and S-waves; OR, outer radius; IF, inner fluid; OF, outer fluid; D, density; F1 and F2 are the formation properties for two fast formations that we investigated; S is a slow formation; and C12, C22, and C32 are the properties of collars that we investigated (C32 is a steel collar). The ∞ is an infinite number.

	V_P (m/s)	Q_p	V_S (m/s)	Q_s	D (g/cm^3)	OR (mm)
IF	1470	100	—	—	1.00	27
OF	1470	100	—	—	1.00	117
F1	4500	50	2650	60	2.30	∞
F2	3000	50	1800	60	2.00	∞
S	2300	50	1000	60	2.00	∞
C12	10,000	∞	6000	∞	7.85	90
C22	8000	∞	5000	∞	7.85	90
C32	6000	∞	3300	∞	7.85	90

SIMULATIONS AND DATA ANALYSIS

Effects of collar properties on the monopole ALWD wavefield in fast formations

We use the DWI method to simulate the waveforms for a multipole ALWD tool in different formations. The source-time function is a Ricker wavelet, whose frequency-domain representation is as follows:

$$S(\omega) = \left(\frac{\omega}{\omega_0}\right)^2 e^{-(\omega/\omega_0)^2}, \quad (1)$$

where ω is the frequency and ω_0 is the source center frequency.

We first discuss the ALWD wavefield in fast formations (F1 and F2 in Table 1). The waveforms are simulated for a monoplole ALWD tool at 10 kHz. The steel collar (C32 in Table 1) is used here.

Figure 2a shows array waveforms for the monopole ALWD tool in F1. We can clearly discern the collar, S, pseudo-Rayleigh (pR), and the Stoneley (ST) waves. The waveforms of the first 1.2 ms are amplified and displayed by the dashed line above the main traces. Figure 2b shows a velocity-time semblance plot for the waveforms. We can see that the P-wave is submerged in the collar wave due to the short spacing in the ALWD tool, which makes it difficult to determine the P-velocity (Aron et al., 1994, 1997; Minear et al., 1995; Joyce et al., 2001; Leggett et al., 2001; Tang et al., 2002). This collar-wave interference needs to be eliminated to analyze the P-wave. Figure 2c shows phase and group velocity dispersion curves for different modes including the collar, pR-, and ST-waves. The collar wave exhibits a strong dispersion for frequencies higher than 10 kHz, which corresponds to the most effective excitation band and the velocities extend over a large range that covers most P-wave velocities in fast formations and makes P-velocity measurement difficult.

We also simulated the response of the monopole ALWD tool in a fast formation F2. The waveforms are shown in Figure 3a, and the waveforms of the first 1.5 ms are amplified and displayed by dashed lines as before. The arrivals of collar, S- pR-, and ST-waves can be discerned clearly, and an obvious arrival appears, which corresponds to the P-wave according to the velocity analysis shown in Figure 3b. The dispersion curves of different modes are shown in Figure 3c. The pR-wave has a higher cutoff frequency compared with that in Figure 2c. We find that the velocity range of the collar wave is well above the P-wave velocity in formation F2 (3000 m/s), and this makes the determination of P-wave possible.

To help us understand the modes propagating in the two different formations, F1 and F2, we use a finite-difference method (Wang et al.,

2013b, 2015) to get wavefield snapshots at 0.7 ms for the two formations (as shown in Figure 4). The upper snapshot is for F1 and the lower is for F2. A monopole source located at (0, 0) in the *x*-*z* profile is used. The collar mode is in the region outlined by the dashed rectangle. It is clear that the collar wave propagates as the fastest mode and the ST mode is the slowest mode. We can see the P-wave in formation F1, but it cannot be measured in the borehole because it is submerged within the extensional collar

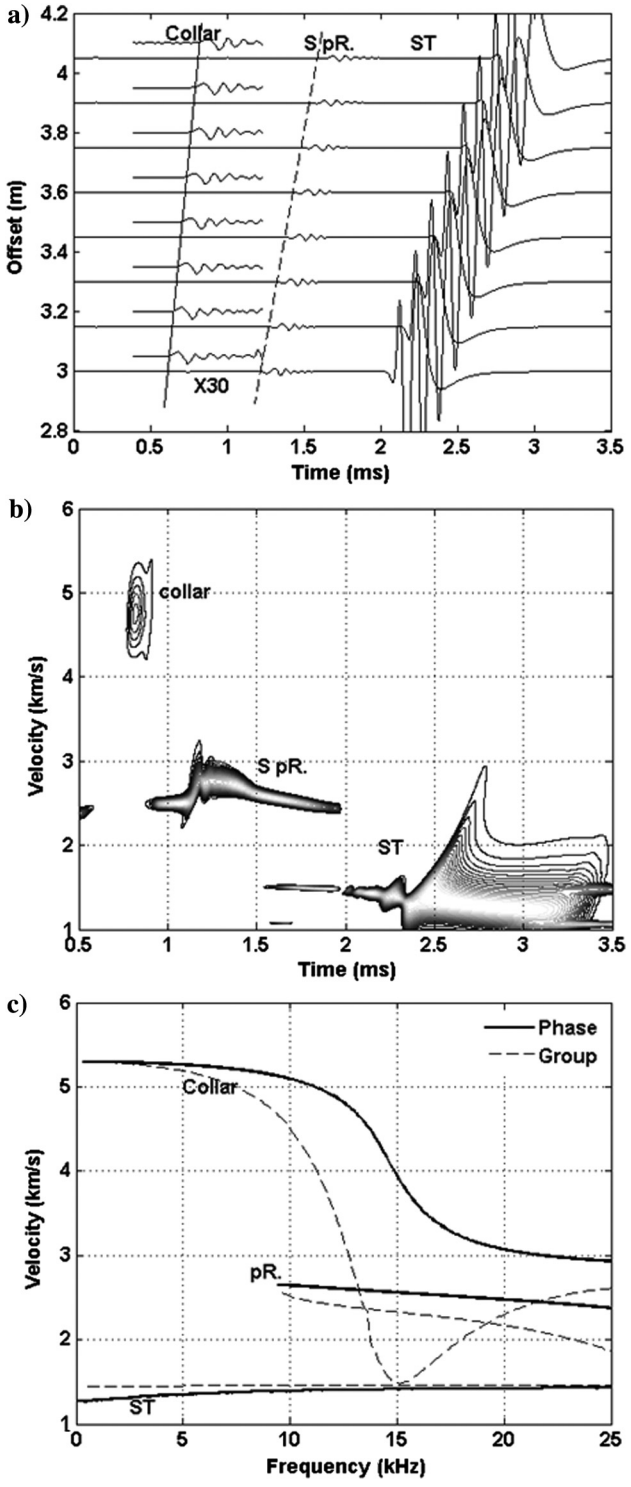

Figure 2. Logging response of a monopole ALWD tool in F1. Parameters of the collar are given as C32 in Table 1. (a-c) The array waveforms, the velocity-time semblance plot, and dispersion curves, respectively. The waveforms of the first 1.2 ms are amplified and displayed by the dash line above the complete traces in panel (a).

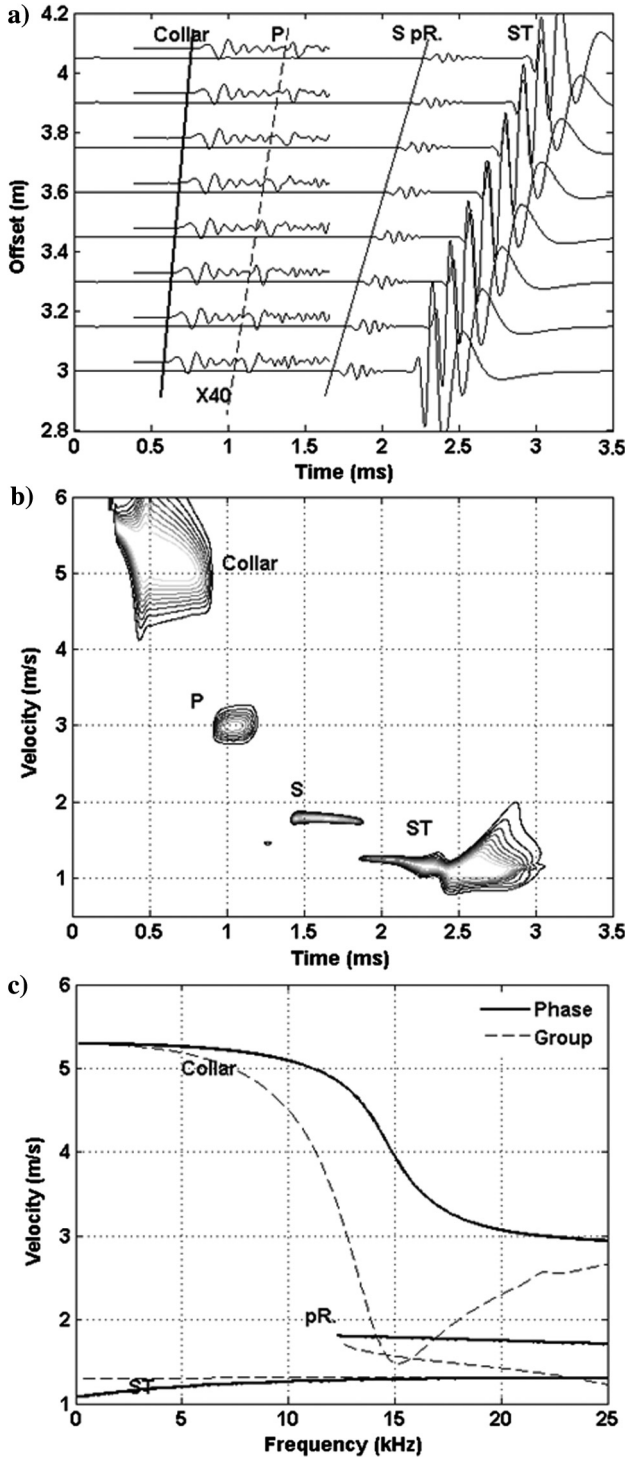

Figure 3. Logging response of a monopole ALWD tool in F2. Parameters of the collar are given as C32 in Table 1. Like Figure 2, except for formation F2 (Table 1).

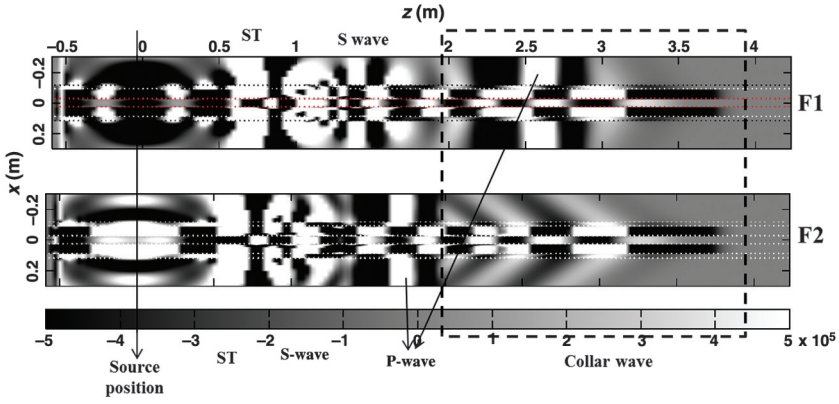

Figure 4. Pressure snapshot at 0.7 ms for the wave propagating in the two different formations with the same LWD monopole tool (C32 in Table 1 for the collar). Upper and lower snapshots are for formations F1 and F2, respectively. Dashed white lines indicate the positions of the inside and outside of the collar.

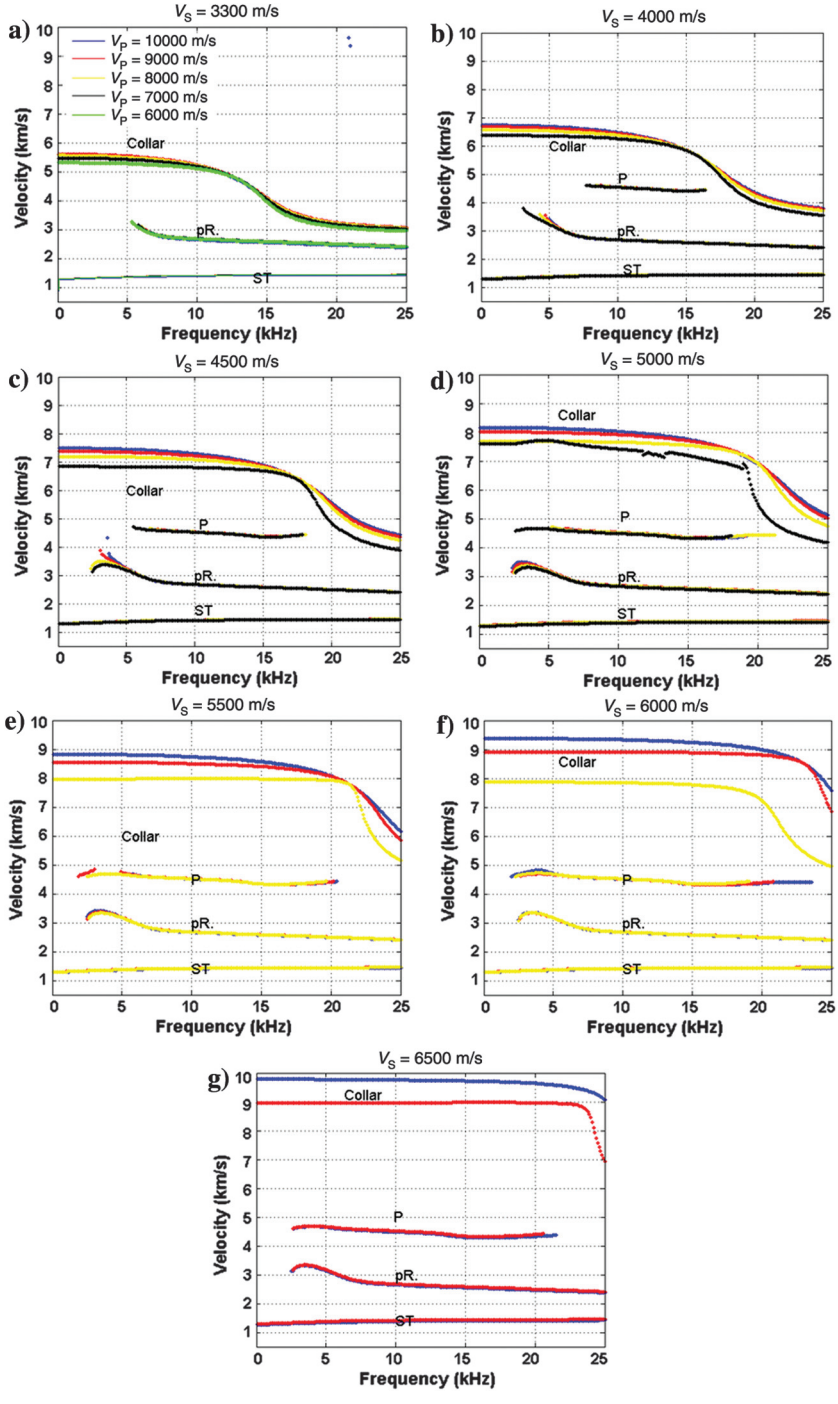

Figure 5. Dispersion curves for monopole ALWD wavefield with various collar compressional velocities for different collar shear velocities. Collar shear velocity is listed above each plot. Legend color for different collar compressional velocities is labeled in panel (a). Formation is F1 (see Table 1).

wave (the upper panel of Figure 4).The S and pR modes follow the collar wave immediately in the borehole for the F1 case. The situation is totally different for F2, where the P-wave clearly appears in the borehole and the S and pR modes propagate slower than in the F1 case.

Our observations from the two simulations discussed above lead us to conclude that if the velocity range of the standard-collar wave is far larger than the formation P-wave velocity, it is possible to direct identify the P-wave without the need for isolators on the collar. However, the velocity range of the collar wave covers the likely range of P-velocities in most fast formations. To see the P-wave, we must make changes to the collar. We will now investigate the influences of different collar properties including velocity, attenuation, and density on the monopole LWD wavefield.

The effects of collar properties on dispersion curves

We investigate the effects of the velocity of the collar wave on the monopole ALWD wavefield by changing the P and S velocities of the collar. Dispersion analysis is a good tool to help us understand the effects of collar velocities, density, and attenuation on the wavefield.

Figure 5 shows the dispersion of the monopole ALWD wavefield for a range of collar velocities, densities, and attenuation factors. The figures show how the dispersion changes with the collar P-wave velocity, when the collar S-wave velocity is 3.3 (Figure 5a), 4 (Figure 5b), 4.5 (Figure 5c), 5 (Figure 5d), 5.5 (Figure 5e), 6 (Figure 5f), and 6.5 km/s (Figure 5g). The color legend for the collar P-wave velocity is shown in Figure 5a.

The dispersion curves of collar, pR-, and ST-waves can be discerned clearly in Figure 5. We find a trend in which the influence of collar compressional velocity on the dispersion curves of the collar wave is not strong when the collar shear velocity is constant. However, the influence of collar compressional velocity on collar wave dispersion curves becomes obvious when the collar shear velocity changes. The collar density and attenuation have little impact on the dispersion. Collar properties do not affect the dispersion of pR- and ST-waves. However, a mode (denoted as P in the figures) propagating with formation P-velocity appears, when the collar shear velocity is larger than 4000 m/s. The mode marked by "P" in Figure 5 is not exactly the P-wave because the P-wave is nondispersive, and the mode in the figure shows slight dispersion. As shown in Figure 4, the collar extensional mode leaks energy into the formation. We thus identify the mode in Figure 5, as being a combination of the formation P-wave and some leaky collar extension mode that has small amplitude, which makes the mode dispersive.

Figure 6 shows dispersion for various collar shear velocities, when collar compressional velocities are 10 (Figure 6a), 9 (Figure 6b), 8 (Figure 6c), and 7 km/s (Figure 6d). The dashed blue, red, yellow, black, jasper, magenta, and green lines are for collar shear velocities of 6.5, 6, 5.5, 5, 4.5, 4, and 3.3 km/s, respectively. It is obvious that the phase velocity of the collar wave is reduced with decreasing collar shear velocity and the P-wave disappears when the collar shear velocity is less than 4 km/s. The pR- and ST-waves are not affected by the collar shear velocity.

To further illustrate the influence of collar properties on the dispersion, we now show the dispersion of the monopole ALWD wavefield in fast formation F2. Following the F1 case, we investigate the effect of collar velocities and density on mode dispersion (as shown in Figures 7 and 8).

Figure 7 shows the dispersion of the monopole ALWD wavefield in F2 for various collar velocities. The figures show that the dispersion changes with the collar compressional velocity when the collar shear velocity is 3.3 (Figure 7a), 4 (Figure 7b), 4.5 (Figure 7c), 5 (Figure 7d), 5.5 (Figure 7e), 6 (Figure 7f), and 6.5 m/s

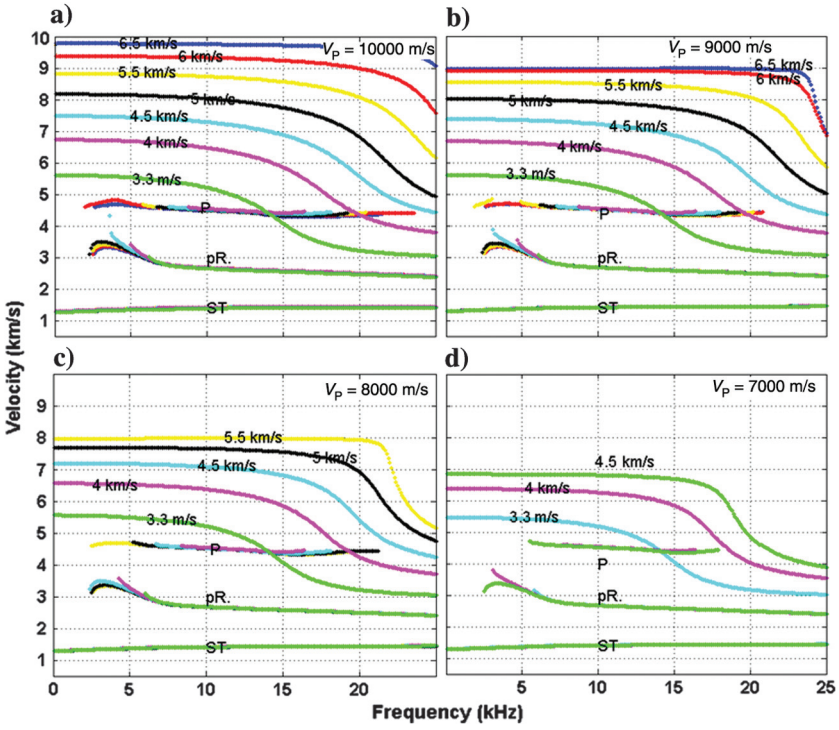

Figure 6. Dispersion curves for monopole ALWD wavefield with various shear velocity for different collar compressional velocities. Collar P-velocity is listed above each plot. The dashed blue, red, yellow, black, jasper, magenta, and green lines are for collar shear velocities of 6500, 6000, 5500, 5000, 4500, 4000, and 3300 m/s, respectively. Formation is F1 (see Table 1).

(Figure 7g). The collar, P-, pR-, and ST-waves can be clearly discerned in Figure 7. We find the same trend as found for model F1: For constant collar shear velocity, the influence of changing collar compressional velocity on the dispersion of the collar wave is not strong. The collar density changes the dispersion very little. Collar properties do not affect the dispersion of pR- and ST-waves.

Figure 8 shows dispersion curves for various collar V_S, when collar V_P are 10 (Figure 8a), 9 (Figure 8b), 8 (Figure 8c), and 7 km/s (Figure 8d). It is obvious that the phase velocity of the collar wave is reduced with reductions in the collar shear velocity. The pR- and ST-waves are not affected by the collar shear velocity. We investigated the influence of the collar density and attenuation factors on the dispersion curves and found very little influence.

Therefore, the collar shear velocity is a key parameter to control the dispersion and phase velocity of the collar wave. If the collar S-wave velocity is larger than 4 km/s, we can easily identify the P-wave for general fast formations.

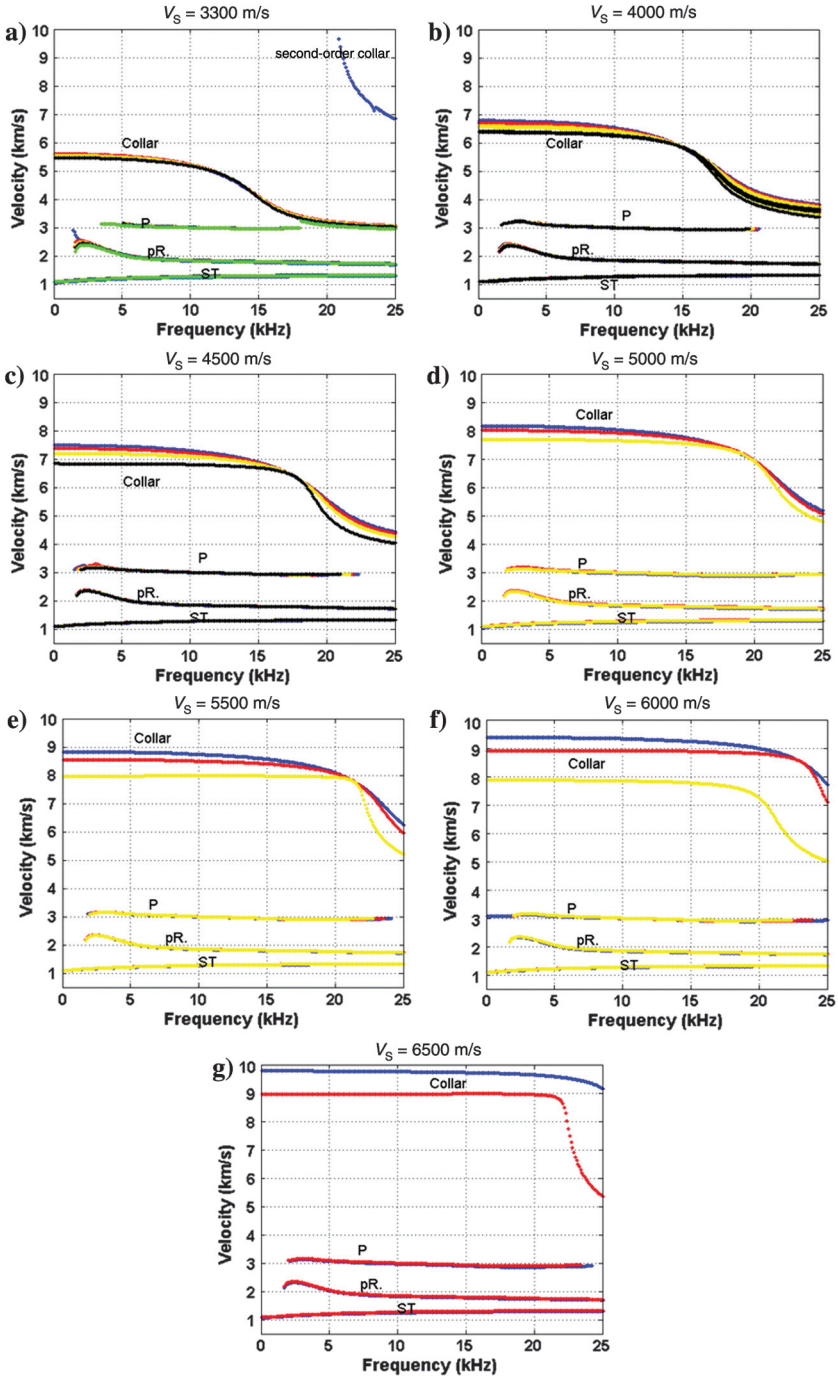

Figure 7. Dispersion curves for monopole ALWD wavefield with various collar compressional velocities for different collar shear velocities. Collar shear velocity is listed above each plot. Lines are color coded as in Figure 5. Formation is F2 (see Table 1).

The effects of collar properties on waveforms

Larger attenuation in the collar has been used to simulate the effect of an isolator that can reduce the amplitude of the collar wave (Wang and Tao, 2011). It is not necessary to discuss this here.

We now consider the effect of collar velocity and density on waveforms. Collars C12, C22, and C32 (in Table 1) are used for the waveform simulations. The collar velocities are set using C12 and four densities are used: 9.0, 7.85, 4.00, and 1.60 g/cm^3. We do not consider attenuation in the collar, and we will use fast formation F1. Figure 9 shows the waveforms for the cases of different collar densities. Figure 9a shows the collar and P-waves, and Figure 9b shows the S-, pR-, and ST-waveforms. The source frequency used here is 10 kHz.

The amplitudes of different modes reduce with increasing collar density. Amplitudes of collar and ST-waves are most strongly influenced by the collar density. The S- and pR-waves are only slightly affected by the density. The influence of the collar density on the ST-wave is mainly exhibited on the arrival time, which advances with increased density. The P-wave amplitude also reduces with increased collar density, but it becomes more obvious and easier to identify due to the significantly reduced amplitude of the collar wave as density increases. Velocity analyses of P-waves for different collar densities are shown in Figure 9c by using contour plots for the density of 1.60, 4.00, 7.85, and 9.00 g/cm^3. It is clear that the coherence of the P-wave on the array receivers becomes stronger and the determination of P-velocity is much easier when the collar density increases.

In the same way, Figure 10 shows the waveforms when the collar velocities are as C22 for different densities. Although we can still discern the P-wave in the array waveforms when the densities are 9.00 and 7.85 g/cm^3, it is obvious that reducing the collar velocities (compare with C12) makes the collar and P-waves arrive much closer in time, which makes the determination of the P-wave difficult. The effects of collar density on the other modes show the same trend as for the C12 case (in Figure 9). However, changes in the S- and pR-waves become more obvious.

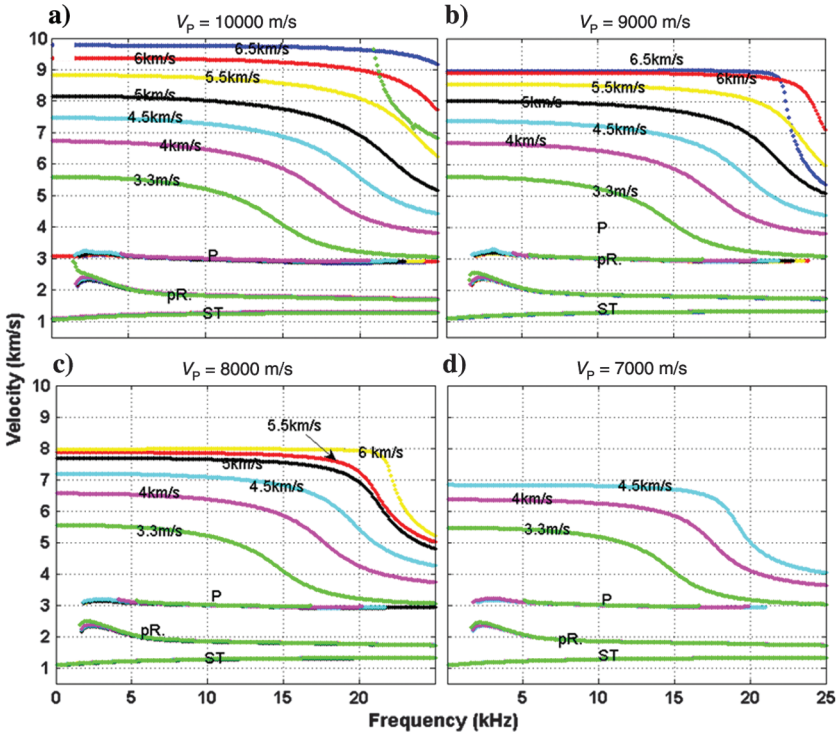

Figure 8. Dispersion curves for monopole ALWD wavefield for different collar P-velocities with different collar compressional velocities. Collar P-velocity is listed above each plot. Lines are color coded as in Figure 6. Formation is F2 (see Table 1).

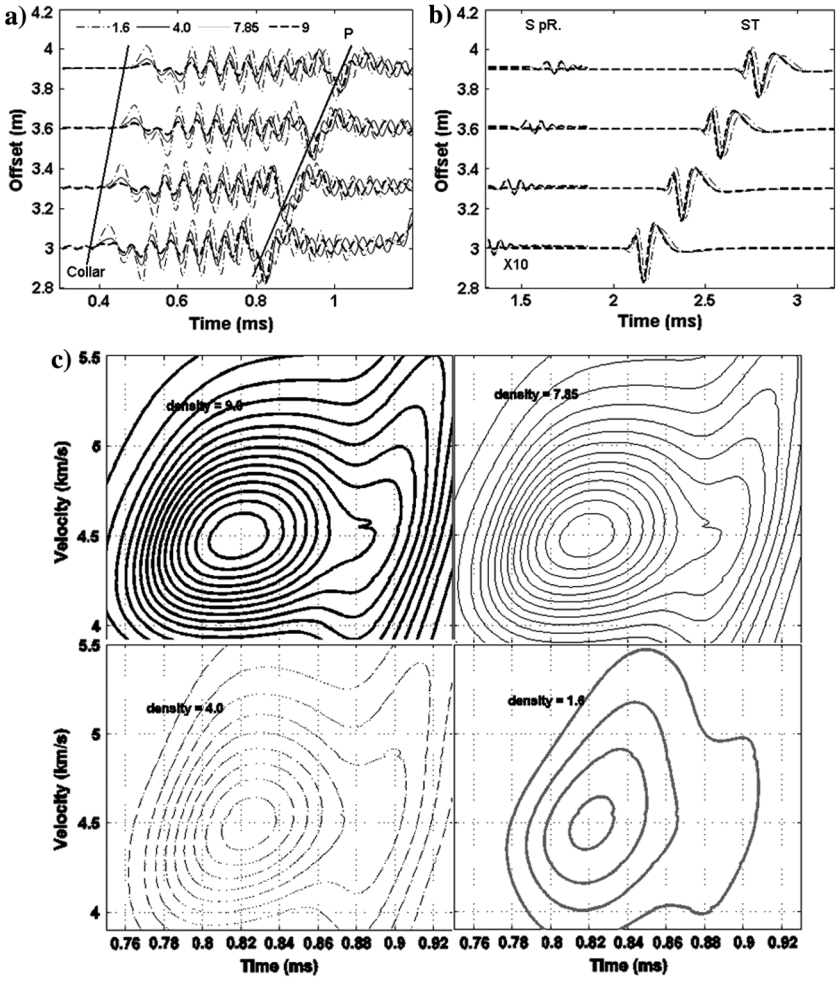

Figure 9. Effect of collar density on waveforms for C12 in formation F1. The dashed-dotted, black solid, gray solid, and dashed lines indicate collar density of 1.60, 4.00, 7.85, and 9.00 g/cm^3, respectively. (a) Collar and P-waves; (b) S-, pR-, and ST-waves; and (c) velocity analysis in contour plots for the array waveforms with the collar density of 1.60, 4.00, 7.85, and 9.00 g/cm^3, respectively.

As discussed above, a larger collar density makes the P-wave much more obvious and easier to pick up. Therefore, it is better to choose a collar density to be as large as possible. Waveforms with collar parameters of C12, C22, and C32 in fast formation F1 are plotted as overlapping lines in Figure 11 to investigate the influence of collar velocity on the waveforms. Figure 11a shows waveforms of the first 1.2 ms, which gives detail about the collar waves from the simulations for three different collars. The black- and gray-filled traces correspond to collars with properties C12 and C22, respectively. We plot only one trace for C32 (dashed line) at 3 m offset. From these three different waveforms at different offsets, we find that the collar-wave frequency increases with collar velocity. Figure 11b shows the pR- and ST-waves.

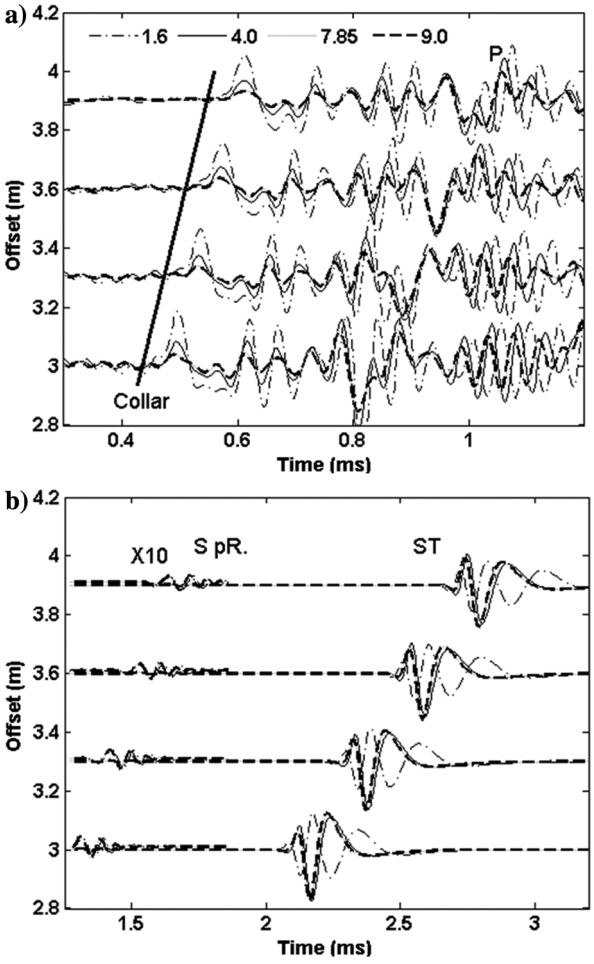

Figure 10. Effect of collar density on waveforms for C22 in formation F1. Density of 1.60, 4.00, 7.85, and 9.00 g/cm^3 cases are labeled as 1.6, 4.0, 7.85, and 9.0, respectively. (a) Collar and P-waves and (b) S-, pR-, and ST-waves.

A P-wave appears, when collar velocities increase from C32 (dashed line in Figure 11a) to C22 (gray filled), and it separates much more from the collar wave when the parameters of the collar become C12 (black filled). Compared with C32, the relatively high frequency and low amplitude of the collar wave makes the P-wave apparent in C12 and C22. However, the collar velocity has little influence on the pR- and ST-waves (Figure 11b).

Effects of collar properties on the dipole ALWD wavefield in a slow formation

Wang and Tao (2011) discuss the data-acquisition scheme in very slow formations for tools with a conventional collar. They find that due to the large velocity difference between the formation and collar flexural waves, the velocity of P- and S-waves can be determined using measurements from a dipole ALWD tool in very slow formation. This implies that when the velocity of the collar is large enough, the dipole collar wavefield in a slow formation changes significantly. It is thus necessary to investigate the effect of collar properties on the dipole wavefield in slow formations. We will now study how collar properties including velocities, density, and attenuation influence the dipole ALWD wavefield. We will also investigate the influence of the collar geometry on the collar flexural wave. Collar geometry is important because the collar flexural rigidity is proportional to its Young's modulus and the difference between the fourth power of collar outer and inner radii (Love [1952], p. 129–130).

The effects of collar properties on dispersion curves

We will first discuss in detail the effects of density and velocity on dispersion curves in a slow formation. The borehole geometry and formation *S* parameters are given in Table 1.

Figure 12 shows the dispersion of the dipole ALWD wavefield for various collar velocities. Collar shear velocity is listed above each plot. Lines are color coded as in Figure 5. We can clearly discern the formation flexural, leaky P-waves and the first-, second-, and third-order collar flexural waves in the figures. The first-order collar flexural wave interferes with the leaky P and the formation flexural waves in the low-frequency band (approximately 6 kHz for the leaky P-wave and 2 kHz for the formation flexural wave), which makes the determination of P and S velocities in the slow formation from leaky P and flexural waves difficult. For the same collar shear

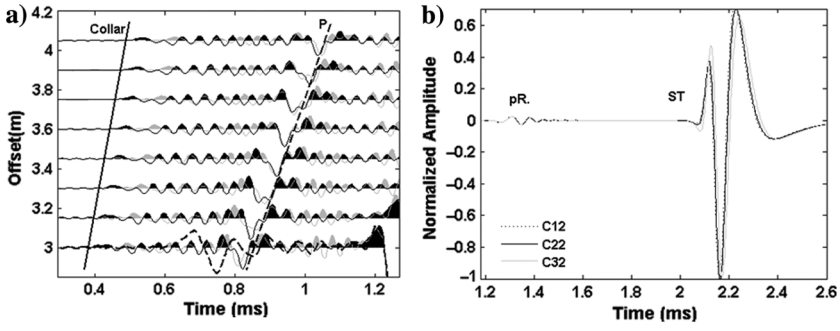

Figure 11. The logging response of a LWD acoustic tool in formation F1. Collars are C12, C22, and C32. (a) First 1.2 ms waveforms, the black- and gray-filled waveforms are corresponding to C12 and C22, respectively; (b) the pR- and ST-waves.

velocity, the influence of changing collar compressional velocity on the dispersion of collar flexural wave is not strong. However, when collar shear velocity increases, the cutoff frequencies of the second- and third-order collar flexural modes increase and the gap between those two modes becomes larger. Collar properties do not affect the dispersion of leaky P and formation flexural waves, but the interference between the first-order collar flexural wave and those two modes becomes weaker with increasing collar S-wave velocity. The decreasing interference is more obvious for the leaky P-wave. We can easily get the formation P-velocity at the cutoff frequency of

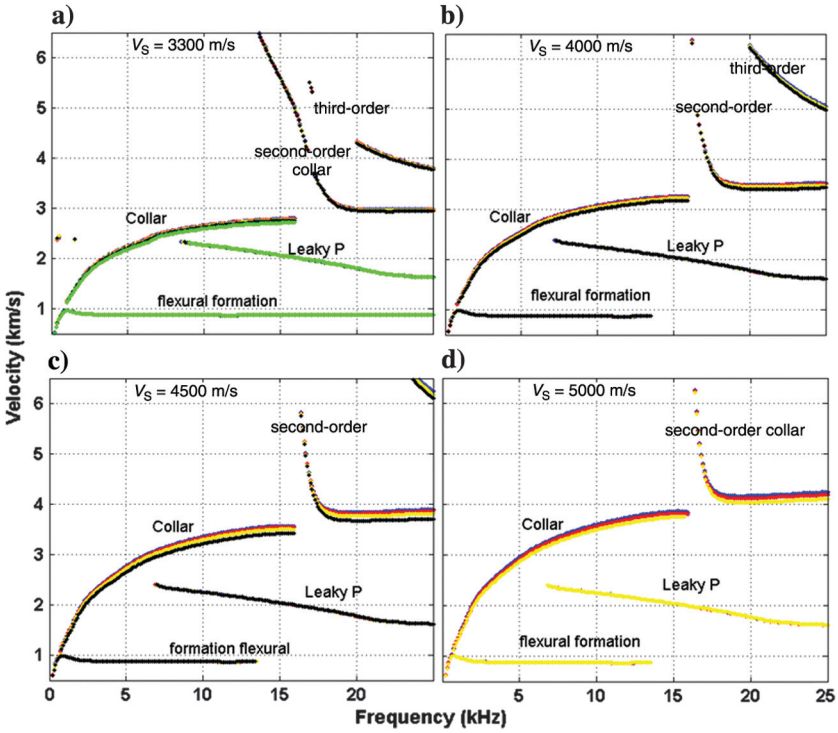

Figure 12. Dispersion curves for dipole ALWD wavefield with various collar compressional velocities for different collar shear velocities. Collar shear velocity is listed above each plot. Lines are color coded as in Figure 5. Formation is *S* (see Table 1).

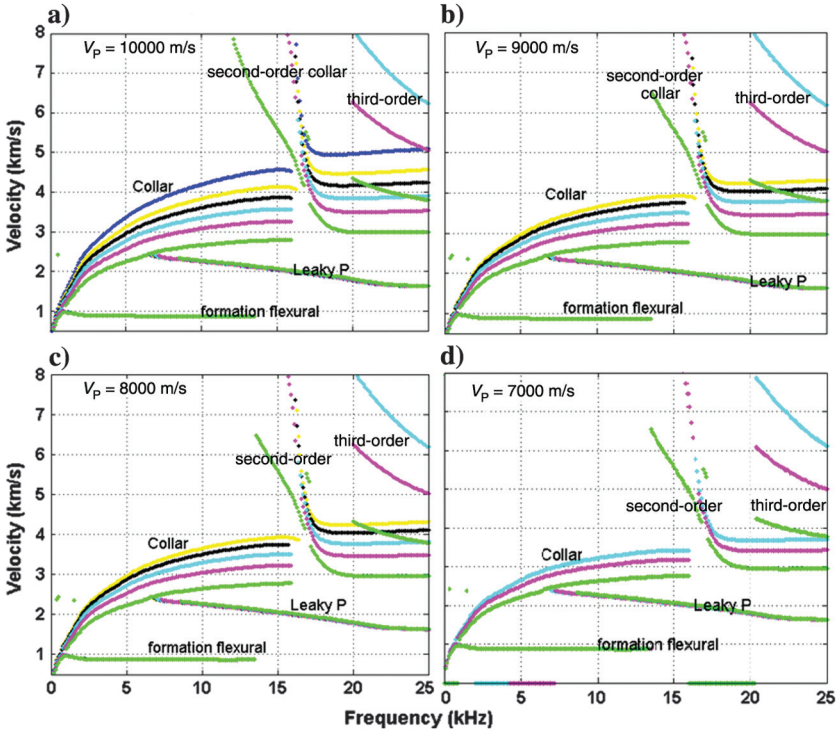

Figure 13. Dispersion curves for dipole ALWD wavefield for various shear velocities with different collar compressional velocities. Collar compressional velocity is listed above each plot. Lines are color coded as in Figure 6. Formation is *S* (see Table 1).

the leaky P-wave, when the collar shear velocity is larger than 4.5 km/s. We can also get the formation *S*-velocity from the formation flexural wave at low frequency.

Figure 13 shows dispersion curves for various collar shear velocities, when collar compressional velocities change. Collar compressional velocity is listed above each plot. Lines are color coded as in Figure 6. It is obvious that the phase velocity of the collar flexural wave increases with increasing collar shear velocity for the same collar compressional velocity. Figures 12 and 13 lead us to understand the factors that control the collar flexural velocity. For a given geometry, the collar flexural rigidity is proportional to the Young's modulus (Love [1952], p. 129–130), which can be determined from the compressional and shear velocities as well as density. The collar density changes the dispersion very little. From the characteristics of flexural collar dispersion curves in Figures 12 and 13, we see that the compressional and shear velocities of the collar affect the collar flexural velocity. However, the collar shear velocity is the key and dominant factor controlling the collar flexural velocity.

The leaky P and formation flexural waves are not affected by the collar shear velocity. The interference from the first-order collar flexural wave on the leaky P and formation flexural waves becomes weaker when the collar shear velocity increases. It is obvious that the cutoff frequency of the leaky P-wave can be discerned when the collar shear velocity is larger than 4.5 km/s (as shown in Figure 13d). Furthermore, if the collar compressional velocity is larger than 7 km/s, the corresponding shear velocity needs to be larger than 4 km/s (as shown in Figure 13a–13c) to allow a clear identification of the leaky P-wave cutoff frequency.

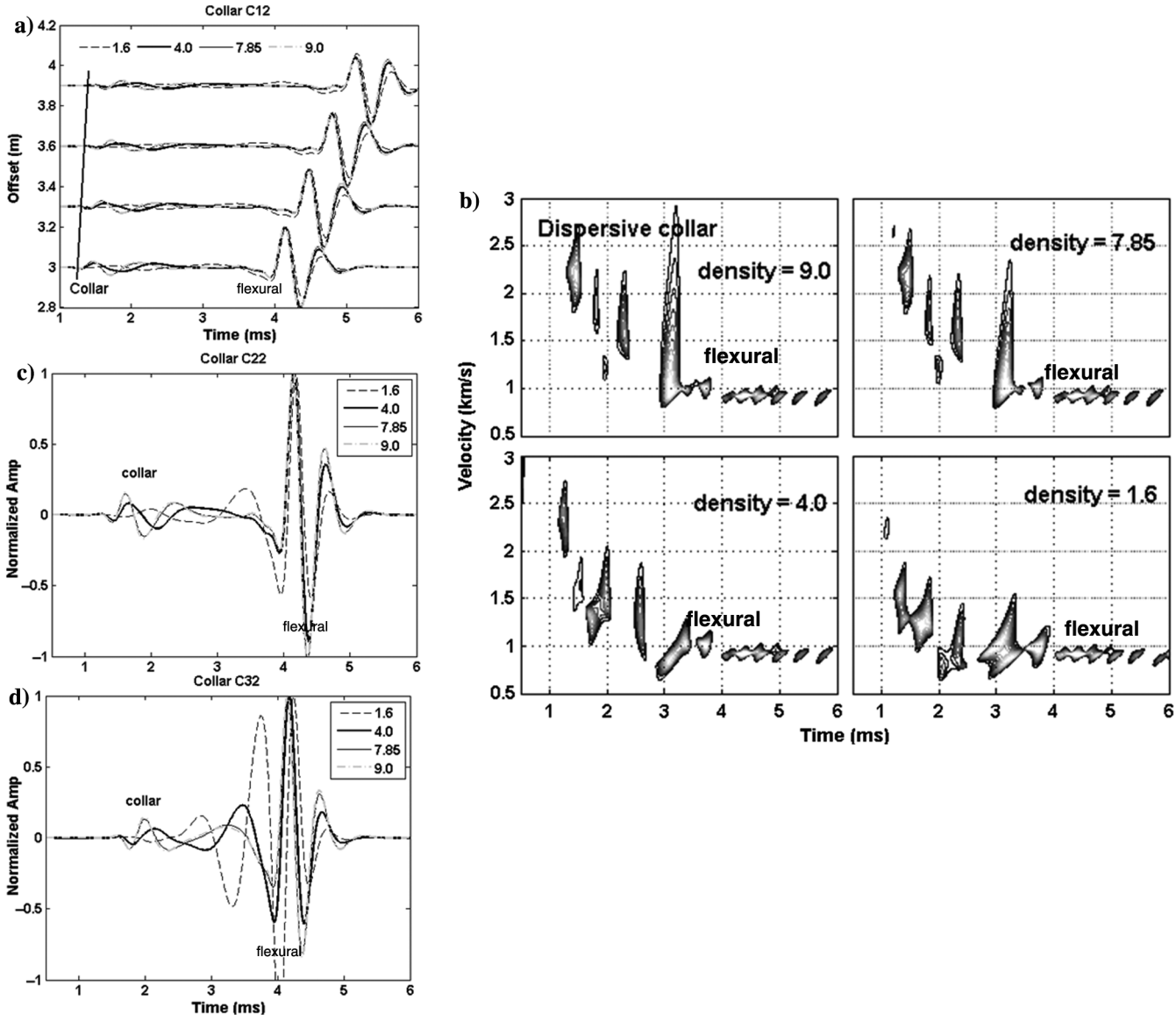

Figure 14. Effect of the collar density on waveforms. (a) Array waveforms for the collar C12 with different densities; (b) velocity analysis for the array waveforms in panel (a); and (c and d) waveforms (offset of 3 m) for the collars C22 and C32 with different densities, respectively. Formation is slow formation *S* (see Table 1). The source frequency used here is 2 kHz. The offset is 3 m in (c and d).

The effects of collar properties on waveforms

We now consider how collar velocity and density affect the waveforms. Collars C12, C22, and C32 (in Table 1) with different densities (9.0, 7.85, 4.0, and 1.6 g/cm^3) were used for waveform simulations of a dipole ALWD tool in slow formation *S*. The source frequency used here is 2 kHz. Figure 14 shows the waveforms for the different density cases. Figure 14a shows the array waveforms for the collar C12 with different densities. The modes' amplitudes increase with increasing collar density, which is different from the monopole case (Figures 9 and 10). However, the effect of density on the waveforms is almost the same: higher density leads to a weaker interference of the collar flexural wave on the formation flexural wave, which will aid in the determination of S-velocity from the flexural wave. We use the semblance method to get velocity information from the array waveforms shown in Figure 14a. The results (in Figure 14b) show a better semblance for the formation flexural wave (a region approximately 1 km/s and 3 ms) with the higher collar density

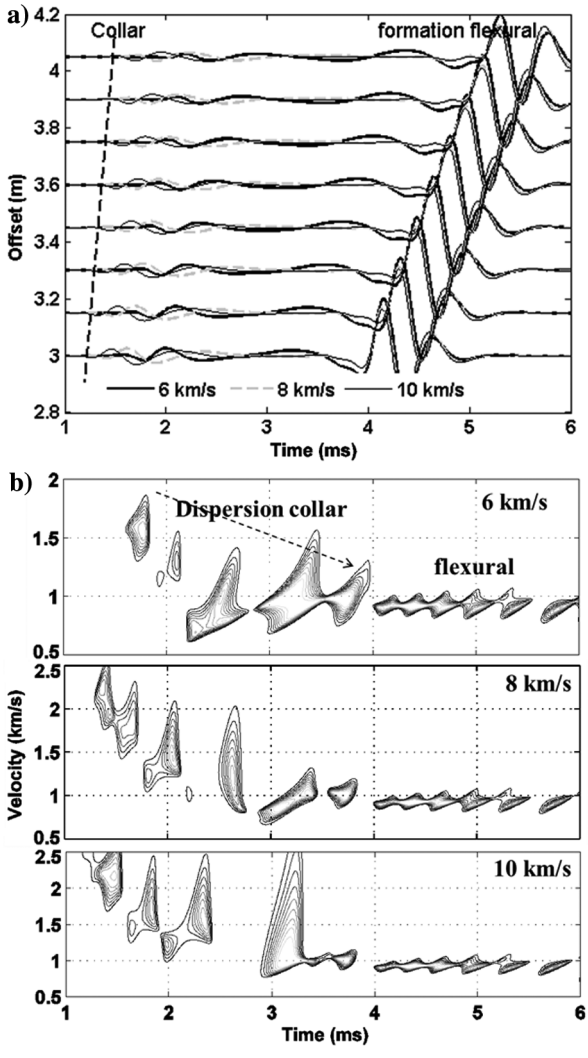

Figure 15. The logging response of the dipole LWD acoustic tool in a slow formation *S*. (a) Array waveforms for the slow formation. Different curves indicate collars with different properties; (b) velocity analysis results for array waveforms.

We also simulated the waveform (3 m offset) for the collar C22 and C32 with different densities, and show results in Figure 14c and 14d, respectively. The influence of density on the waveforms appears stronger than for the C12 case where the collar velocity is larger than those of C22 and C32. We cannot distinguish the ending time of the collar wave and the starting time of the formation flexural wave due to the long duration of the collar wave when the density is 1.6 g/cm^3. The small density collar results in a long duration collar wave, which makes the determination of the S-velocity from the formation flexural wave difficult especially for the case of a collar with a low velocity.

To investigate the influence of collar velocities on dipole waveforms, we show array waveforms for collars C32, C22, and C12 in the slow formation *S*. Figure 15a shows the array waveforms for the collars, where the thick, gray dashed, and thin lines are for collars C32, C22, and C12, respectively. We find distinct collar and formation flexural waves. The collar flexural waves disturb the formation flexural waves to some extent. When collar velocity increases, the interference becomes weaker and the arrival of the formation flexural wave can be determined clearly when the compressional and shear velocities of the collar are 10 and 6 km/s, respectively. The velocity-time semblance plots (Figure 15b) show that the velocity of the dispersive collar wave ranges from 1.3 to 3 km/s, and the velocity of the formation flexural wave is less than 1 km/s. However, the velocities of formation flexural wave approach the formation shear velocity, when the collar velocities increase because the interference between the collar and the formation flexural waves becomes weaker. We can easily determine the shear velocity from the dispersion of flexural waves at low frequency (approximately 2 kHz) using the dipole ALWD tool in slow formations because the interference between the collar and formation flexural waves becomes weaker when the collar velocities increase.

Based on our observations from the models shown, we conclude that a collar with large velocities (especially one with the shear velocity more than 4 km/s) and large density will enable the dipole tool to measure the formation P and S velocities for all slow formations. This also applies for very slow formations.

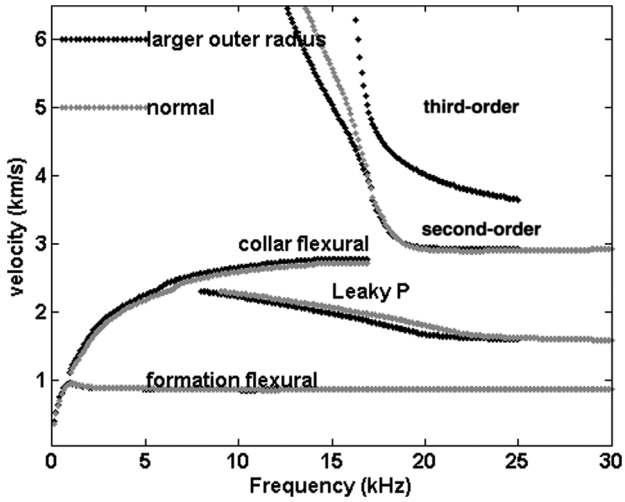

Figure 16. Dispersion curves for collar with properties C32 in slow formation *S* for collars with two different geometries.

Influence of collar pipe geometry on the dipole ALWD wavefield in a slow formation

As previously stated, Love's principle (Love [1952], p. 129–130; Poletto and Miranda [2004], p. 82) says that the collar flexural rigidity is a function of the difference between the fourth power of inner and outer radii of the collar when velocity and density of the collar are held constant. The geometry of the models used in the simulations discussed above is appropriate for a 9.21 in borehole. However, in real ALWD applications, slim and large boreholes will also be encountered and the radii, especially that of the outer radius, of collar will change. Here, we only increase the outer radius of drill pipe to be 100 mm and the borehole radius to be 127 mm to consider the large borehole case and investigate the effect of collar geometry on the wavefield. The dispersion curves of collar C32 for different geometries are shown in Figure 16. The black points are for the modes from the large borehole model, and the gray ones are for the normal size model. We find that the collar flexural velocity becomes larger than that the normal size case and the third-order collar flexural mode appears when the outer radius of the collar increases. The enlarged outer radius makes the flexural rigidity larger and the

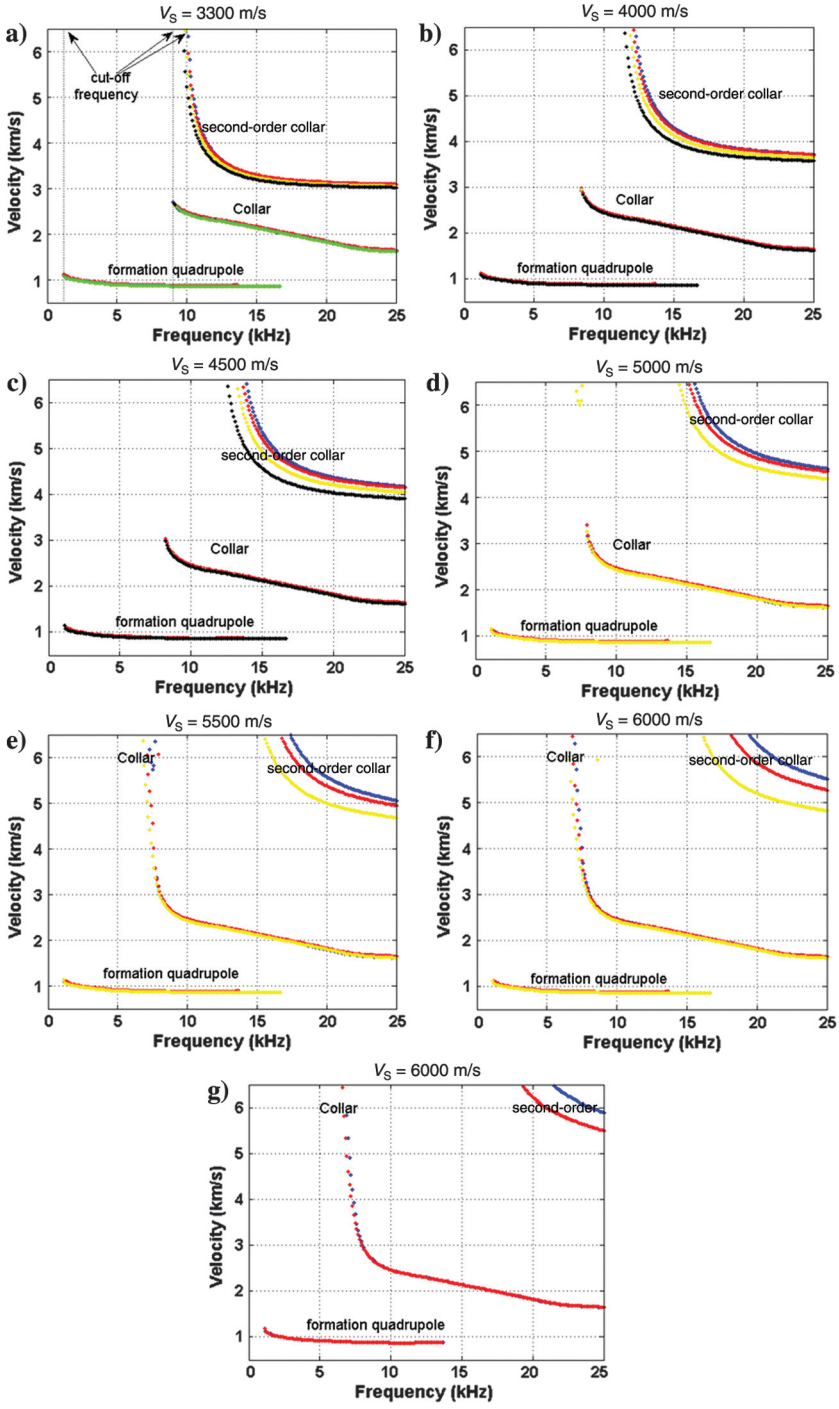

Figure 17. Dispersion curves for quadrupole ALWD wavefield with various collar compressional velocities for different collar shear velocities. Collar S-wave velocity is listed above each plot. Lines are color coded as in Figure 5. Formation is *S* (see Table 1).

effect of the collar flexural wave on the formation modes becomes weaker than those in the normal size drill collar case. However, the difference between the normal and the larger size collars is not too large.

Effects of collar properties on the quadrupole ALWD wavefield in a slow formation

Due to the interference of the collar flexural wave on the low-frequency formation flexural wave from a dipole tool, a quadrupole ALWD tool is used in industry to acquire shear velocities in slow formations (Tang et al., 2002). It is thus necessary to investigate the effects of the collar properties on the quadrupole ALWD wavefield in slow formations. Following the approach taken for the monopole and dipole cases, we calculate the dispersion curves of borehole modes for the quadrupole ALWD tool in a slow formation. For various collar densities and velocities, we use the slow formation *S* given in Table 1.

Figure 17 shows the dispersion of the quadrupole ALWD wavefield for a suite of collar velocities. The results show that the dispersion changes with changes in the collar compressional velocity when the collar shear velocity is fixed as shown in each plot. Lines are color coded as in Figure 5. It is easy to discern the formation quadrupole wave as well as the first- and second-order collar quadrupole waves in the figures. All the collar modes have cutoff frequencies that differ from those for the dipole cases. The first-order collar mode and the formation flexural wave do not have a cutoff frequency in the dipole case. There is no interference between the formation and collar waves, and the shear velocity can be easily determined from the velocity of the formation quadrupole mode at its cutoff frequency. For a fixed collar shear velocity, changing the collar compressional velocity does not change the dispersion of the first-order collar wave. However, it changes the higher (second) order modes considerably especially for higher collar shear velocities (Figure 17e–17g). Higher collar compressional velocities lead to larger the cutoff frequencies for the second-order collar wave. However, the cutoff frequency moves to a lower frequency with increased V_S of the collar. The cutoff frequencies of the second-order collar modes also increase with increasing collar shear velocity, and the gap between the first- and second-order modes becomes larger, which is similar to the dipole case. Although the cutoff frequency of the first-order collar wave moves to a lower frequency with increased shear velocity of the collar, which would affect the measurement of formation shear velocity, the formation quadrupole mode is not affected by the collar properties very much.

Figure 18 shows dispersion for various collar shear velocities when collar compressional velocities are 10 (Figure 18a), 9 (Figure 18b), 8 (Figure 18c), and 7 km/s (Figure 18d). Lines are color coded as in Figure 6. It is obvious that the collar properties do not affect the dispersion curves of the formation and first-order collar quadrupole modes very much.

DISCUSSION

Based on the results that we have presented about the influence of collar properties on the ALWD wavefield, we see that the formation P- and S-wave velocities can be reliably determined using a monopole or dipole ALWD tool directly from the monopole measurement without the need for isolators on the drill collar provided that we find a collar material with large velocity and density. It would be desirable if the collar and the shear velocity were more than 4 km/s.

An advanced composite material could be a good option for a collar, particularly for borehole environments with high temperature, high pressure, and high rigidity (Wu, 2000). For example, the aluminum matrix composite reinforced by carbon and silicon carbide fiber can withstand a temperature of 500°C and maintain sufficient rigidity and elastic moduli (Prewo and Brennan, 1980). Alternatively, a silicon carbide fiber combined with titanium would

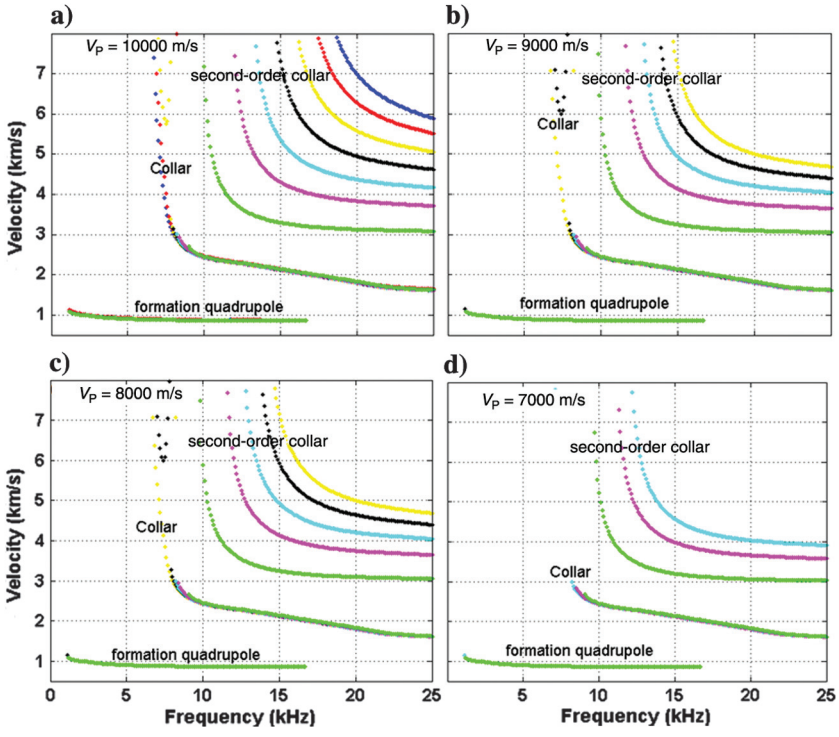

Figure 18. Dispersion curves for quadrupole ALWD wavefield with various shear velocities for different collar compressional velocities. Collar compressional wave velocity is listed above each plot. Lines are color coded as in Figure 6. Formation is *S* (see Table 1).

increase the heat resistance of titanium, so it could withstand wear and tear (Yamamura et al., 1988). The maximum temperature for the tool could reach approximately 1500°C when a silicon carbide fiber is compounded with ceramic (Moezzi et al., 2012). An advanced composite material Al_3O_2 ceramic (Accuratus, 2013) with compressional velocity of 10 km/s and shear velocity of 6 km/s has also been demonstrated. The increased cost of the composite material may be partially offset by the decreased time in tool construction compared with one using a conventional acoustic isolator.

With collars made of well-chosen materials, the velocity of P- and S-waves could then be determined directly by the LWD measurement system. This might be an easy change to implement and lead to a new approach for LWD acoustic tool design.

CONCLUSIONS

In this paper, we have used the wavenumber integration, analytical dispersion calculations, and velocity semblance methods to investigate properties of the collar on multipole ALWD wavefields for fast and slow formations. Our conclusions are as follows:

1) The collar wave interferes with the P-wave, when the difference between the collar and the P-velocities is small. However, the interference disappears with the velocity difference increases.
2) Large density and collar velocities (especially for shear velocity more than 4000 m/s) make the P-velocity determination possible without the need for isolators on the drill collar in fast formations.
3) With increasing collar velocities, the interference between the collar wave and the formation flexural wave can be very slight for a dipole tool in a slow formation, and the S-velocity can be determined by the dispersion of flexural formation wave.

Therefore, we suggest that the use of an advanced composite material that increases the collar velocities and density in the ALWD tool would facilitate the direct measurement of the velocity of the P- and S-waves. This would be an easy change to implement and a new idea for LWD acoustic tool design.

ACKNOWLEDGMENTS

This study is supported by NSFC (nos. 41404100 and 4117411), a China Post-doctoral Science Foundation (no. 2013M530106), and The International Postdoctoral Exchange Fellowship Program. The four anonymous reviewers are deeply appreciated for their critical and constructive comments to this work.

REFERENCES

Accuratus, 2013, Aluminum oxide, Al_2O_3 ceramic properties, http://accuratus.com/alumox.html, accessed 10 April 2016.
Aron, J., S. K. Chang, D. Codazzi, R. Dworak, K. Hsu, T. Lau, O. Minerbo, and E. Yogeswaren, 1997, Real-time sonic logging while drilling in hard and soft rocks: Presented at the SPWLA 38th Annual Logging Symposium, Paper HH.
Aron, J., S. K. Chang, R. Dworak, K. Hsu, T. Lau, J- P. Masson, J. Mayes, G. McDaniel, C. Randall, S. Kosteck, and T. L. Plona, 1994, Sonic compression measurements while drilling: Presented at the SPWLA 35th Annual Logging Symposium, Paper SS.
Byun, J., and M. N. Toksöz, 2003, Analysis of the acoustic wavefields excited by the logging-while-drilling (LWD) tool: Geosytem Engineering, **6**, 19–25, doi: 10.1080/12269328.2003.10541200.
Chen, T., B. Wang, Z. Zhu, and D. Burns, 2010, Asymmetric source acoustic LWD for improved formation shear velocity estimation: 80th Annual International Meeting, SEG, Expanded Abstracts, 548–552.
Joyce, B., D. Patterson, J. Leggett, and V. Dubinsky, 2001, Introduction of a new omni-directional acoustic system for improved real-time LWD sonic logging-tool design and field test results: Presented at the SPWLA 42nd Annual Logging Symposium, Paper SS.
Kimball, C. V., and T. Marzetta, 1984, Semblance processing of borehole acoustic array data: Geophysics, **49**, 274–281, doi: 10.1190/1.1441659.
Kinoshita, T., A. Dumont, H. Hori, N. Sakiyama, J. Morley, and F. Garcia-Osuna, 2010, LWD sonic tool design for high-quality logs: 80th Annual International Meeting, SEG, Expanded Abstracts, 513–517, doi: 10.1190/SEGEAB.29.
Leggett, J. V., V. Dubinsky, D. Patterson, and A. Bolshakov, 2001, Field test results demonstrating improved real-time data quality in an advanced LWD Acoustic system: SPE, 71732.
Love, A. E. H., 1952, A treatise on the mathematical theory of elasticity (4th ed.): Dover Publications.
Minear, J., R. Birchak, C. Robbins, E. Linyaev, B. Mackie, D. Young, and R. Malloy, 1995, Compressional slowness measurements while drilling: Presented at the SPWLA 36th Annual Logging Symposium, Paper VV.
Moezzi, A., A. McDonagh, and M. Cortie, 2012, Zinc oxide particles: Synthesis, properties and applications: Chemical Engineering Journal, **15**, 1–22, doi: 10.1016/j.cej.2012.01.076..
Poletto, F., and F. Miranda, 2004, Seismic while drilling: Fundamentals of drill-bit seismic for exploration: Elsevier Publishing.
Prewo, K., and J. Brennan, 1980, High-strength silicon carbide fibre-reinforced glass-matrix composites: Journal of Materials Science, **15**, 463–468, doi: 10.1007/BF02396796.
Tang, X., and A. Cheng, 2004, Quantitative borehole acoustic methods: Elsevier Press.
Tang, X., T. Wang, and D. Patterson, 2002, Multipole acoustic logging-while-drilling: 72nd Annual International Meeting, SEG, Expanded Abstracts, 364–367.
Varsamis, G. L., L. Wisniewski, A. Arian, and G. Althoff, 1999, A new MWD full wave dual mode sonic tool design and case histories: Presented at the SPWLA 40th Annual Logging Symposium, Paper F.
Wang, H., and G. Tao, 2011, Wavefield simulation and data acquisition scheme analysis for LWD acoustic tool in very slow formations: Geophysics, **76**, no. 3, E59–E68, doi: 10.1190/1.3552929.
Wang, H., G. Tao, and M. Fehler, 2015, Investigation of the high-frequency wavefield of an off-center monopole acoustic logging-while-drilling tool: Geophysics, **80**, no. 4, D329–D341, doi: 10.1190/geo2014-0426.1.
Wang, H., G. Tao, X. Shang, X. Fang, and D. Burns, 2013b, Stability of finite difference numerical simulations of acoustic logging-while-drilling with different perfectly matched layer schemes: Applied Geophysics, **10**, 384–396, doi: 10.1007/s11770-013-0400-6.
Wang, H., G. Tao, B. Wang, W. Li, and X. Zhang, 2009b, Wave field simulation and data acquisition scheme analysis for LWD acoustic tool: Chinese Journal of Geophysics (in Chinese), **52**, 2402–2409.
Wang, H., G. Tao, and X. Zhang, 2009a, Review on the development of acoustic logging while drilling (in Chinese): Well Logging Technology, **33**, 197–203.
Wang, H., G. Tao, and K. Zhang, 2013a, Wavefield simulation and analysis with the finite-element method for acoustic logging while drilling in horizontal and deviated wells: Geophysics, **78**, no. 6, D525–D543, doi: 10.1190/geo2012-0542.1.
Wu, R., 2000, Composite materials: Tianjin University Press.
Yamamura, T., T. Ishikawa, M. Shibuya, and K. Okamura, 1988, Development of a new continuous Si-Ti-C-O fibre using an organometallic polymer precursor: Journal of Materials science, **23**, 2589–2594, doi: 10.1007/BF01111919.
Zhan, X., Z. Zhu, S. Chi, and M. Toksöz, 2010, Elimination of LWD (logging while drilling) tool modes using seismoelectric data: Communications in Computational Physics, **7**, 47–63.